Toward Stable Monolithic Perovskite/Silicon Tandem Photovoltaics: A Six-Month Outdoor Performance Study in a Hot and Humid Climate

Towards stable monolithic perovskite/silicon tandem photovoltaics: A six-month outdoor performance study in a hot and humid climate

Michele De Bastiani,[1,] Emmanuel Van Kerschaver,[1] Quentin Jeangros,[2] Atteq Ur Rehman,[1] Erkan Aydin,[1] Furkan H. Isikgor,[1] Alessandro J. Mirabelli,[1,3] Maxime Babics,[1] Jiang Liu,[1] Shynggys Zhumagali,[1] Esma Ugur,[1] George T. Harrison,[1] Thomas G. Allen,[1] Bin Chen,[4] Yi Hou,[4,5] Semen Shikin,[1] Edward H. Sargent,[4] Christophe Ballif,[2] Michael Salvador,[1] and Stefaan De Wolf[1,*]*

AUTHOR ADDRESS

1 KAUST Solar Center (KSC), Physical Sciences and Engineering Division (PSE), King Abdullah University of Science and Technology (KAUST), Thuwal 23955-6900, Kingdom of Saudi Arabia.
2. Photovoltaics and Thin-Film Electronics Laboratory (PV-lab), Institute of Microengineering (IMT), Ecole Polytechnique Fédérale de Lausanne (EPFL), Rue de la Maladière 71b, CH-2002 Neuchâtel, Switzerland.
3 Current affiliation: Department of Chemical Engineering & Biotechnology, University of Cambridge, Philippa Fawcett Drive, Cambridge CB3 0AS, United Kingdom.
4 Electrical and Computer Engineering, University of Toronto, Toronto, Ontario M5S 1A4, Canada.
5 Current affiliation: Department of Chemical and Biomolecular Engineering, National University of Singapore, 4 Engineering Drive 4, 117585 Singapore

AUTHOR INFORMATION

Corresponding Author

*Michele.debastiani@kaust.edu.sa

*Stefaan.dewolf@kaust.edu.sa

ABSTRACT

Perovskite/silicon tandem solar cells are emerging as a high-efficiency and prospectively cost-effective solar technology with great promise for deployment at the utility scale. However, despite the remarkable performance progress reported lately, assuring sufficient device stability – particularly of the perovskite top cell – remains a challenge on the path to practical impact. In this work, we analyze the outdoor performance of encapsulated bifacial perovskite/silicon tandems, by carrying out field-testing in Saudi Arabia. Over a six month experiment, we find that the open circuit voltage retains its initial value, whereas the fill factor degrades, which is found to have two causes. A first degradation mechanism is linked with ion migration in the perovskite and is largely reversible overnight, though it does induce hysteretic behavior over time. A second, irreversible, mechanism is caused by corrosion of the silver metal top contact with the formation of silver iodide. These findings provide directions for the design of new and more stable perovskite/silicon tandems.

MAIN TEXT

The continuous reduction in manufacturing costs of crystalline silicon (c-Si) solar cells and modules, combined with a steady increase in their performance, has rendered photovoltaics a cost-effective form of electricity generation.[1] With the remarkable development of perovskite solar cells (PSCs), an opportunity has arisen to further reduce the levelized cost of electricity (LCOE) of photovoltaics by combining both technologies to form the monolithic perovskite/silicon multi-junction solar cell configuration.[2-7] This technology has already reached certified power conversion efficiencies (PCEs) exceeding 29%,[7,8] while theoretical predictions based on ideal current matching conditions point to PCEs beyond 32%.[9] This significant progress and promise justifies inclusion of perovskite/silicon tandem technology in the global energy roadmap towards a climate neutral economy.[1]

Challenges on the road to a perovskite/silicon tandem technology include scalability, as well as stability and reliability of devices and modules.[10] Commercial c-Si solar modules usually are sold with a guarantee to retain after 20-25 years at least 80% of their initial power output. For commercial viability, perovskite/silicon modules will have to adhere to such rigorous standards. However, at present, PSCs are still often found to suffer from a rapid performance loss, often induced by environmental conditions such as humidity and light.[11-13] Quantification of device stability usually consists of reporting the performance of PSCs for a set amount of time (typically 1,000 hours) under controlled testing conditions.[10,14]

However, prolonged outdoor exposure entails the presence, often in diurnal and seasonal cycles, of light, moisture, water, heat, wind, and soiling. These factors may simultaneously induce several degradation processes, possibly acting synergistically, that could remain undetected in a standardized lab-test.[15,16] Outdoor testing also requires a reliable encapsulation strategy,

compatible with the relatively sensitive perovskite device stack.[10,17] To date, the performance loss in perovskite-based devices is usually explained by one of the following scenarios, but alternative mechanisms are possible too: *i)* segregation of the perovskite crystal lattice into iodide- and bromide-rich phases, *ii)* light-induced decomposition of the perovskite phase due to redox reactions under the presence of moisture, temperature, and other environmental factors and *iii)* degradation of the metal electrodes and adjacent contact interfaces.[3,18-22]

Previously, we reported outdoor testing of perovskite/silicon tandem solar cells. We found that under sunny and hot climate conditions the ideal bandgap of the perovskite should be lower than 1.68 eV for monofacial tandem devices.[15] More recently, we found that bifacial tandems benefit from an additional reduction of the perovskite bandgap to satisfy current matching conditions in the presence of light reflection from the ground (albedo).[23] A direct consequence of such reduced bandgap requirements is the opportunity to employ perovskites with a lower bromide content, which are less susceptible to halide segregation.[18]

Here we study the diurnal and long-term evolution of encapsulated bifacial perovskite/silicon tandem solar cells over a six months period (December until June) outdoors in a hot and humid coastal area in Saudi Arabia, with specific attention to the photovoltaic parameters and possible degradation pathways. This location is representative for regions with very high solar power densities (~2500 kWh/m^2/yr) and also imposes a significant challenge in terms of high temperatures, humidity and soiling, typical for tropical and desert regions, thereby representing an important test for the robustness of state-of-the-art perovskite/silicon devices. We chose here the bifacial tandem configuration which mandates the use of narrow-bandgap perovskites, implying enhanced device stability thanks to their lower bromide content. Over six months of continuous monitoring, the devices showed negligible variations in open-circuit voltage (V_{oc}) and relatively

small losses in short circuit current density (J_{sc}). The primary performance drop is associated with losses in fill factor (*FF*) for which we identify two underlying causes: *i)* a reversible degradation mechanism that recovers overnight, and *ii)* an irreversible degradation mechanism that monotonically erodes device performance at an approximate rate of 0.06 (mW/cm^2) absolute in power density per day. By reproducing the *FF*'s reversible behavior in a controlled lab environment, and by performing a detailed microscopy analysis, we conclude that ion migration within the perovskite and alteration of the device's top contact are the most likely causes for these reversible and irreversible losses in *FF*, respectively. These findings aid in setting the research agenda to accelerate the market introduction of perovskite/silicon technology.

For this work, we placed three identical bifacial perovskite/silicon tandem solar cells (in the *p-i-n* configuration, built onto textured heterojunction (SHJ) bottom cells, labeled sample A, B, C), as well as a single-junction SHJ control device on a south-facing test-field structure with an inclination of 25°, matching the local latitude. Fig. 1a sketches the layered structure of the tested devices. To satisfy current matching under these bifaciality conditions, the bandgap of the perovskite was set to be 1.59 eV. The performance of the devices before encapsulation is reported in Fig. S1. The initial PCE of the three tandems is ~23%, measured in monofacial mode (*i.e.* without any additional irradiance from the rear side), where the total current and PCE is limited by the lack of photons reaching the silicon sub-cell due to the narrow bandgap perovskite top cell. For protection against environmental agents, we encapsulated the cells under vacuum, sandwiched between two glass sheets sealed with butyl rubber on the edges, as described in detail in the Methods section.[24] Our encapsulation strategy provides a strong barrier against the relatively high and constant level of moisture measured in our test-field location (see Fig. S2). Fig. 1b-1f shows the solar irradiance (Fig. 1b) and the main photovoltaic parameters (Fig. 1c-1f) for one of the

bifacial tandems (sample A) tracked with a *J(V)* curve every ten minutes during the sunlight hours, over a period of six months outdoors (in between the measurements the devices were kept in open circuit condition). For the sake of clarity, we differentiated the data collected in the morning (06:00am-noon, gray) and afternoon (noon-06:00pm, orange). We found that the V_{OC} (Fig 1c), does not give evidence of degradation and retains its initial value over six months of continuous field testing (Fig. S3). As the V_{OC} is directly linked to the optoelectronic properties of the absorber material, we conclude that the perovskite layer, within the device-active area, remains to be intact in its bulk composition and surface passivation. The J_{sc} scales with the solar irradiance for the first five months (Fig. 1d), with some variations due to dust accumulation (Fig. S3). Only during the last month (June) did the rise in the environmental temperature cause the perovskite bandgap to increase and the c-Si to decrease (Fig. S4),[15] resulting in a current mismatch and a decay in J_{sc}. In principle, this loss in J_{sc} could also be partially caused by other mechanisms linked to the degradation of the tandem, which we discuss below. The *FF*, however, shows clear evidence of continuous degradation with initial values close to 80%, which drop to about 50% after six months (Fig. 1e). Moreover, its value exhibits a daily variation with higher morning values (gray) compared to the afternoon (orange). In a separate test-field experiment, we observed a similar behavior in two single-junction PSCs (Fig. S5). As a result, the power density predominantly follows the behavior of *FF*, losing half of its initial value after six months (Fig. 1f). A detailed analysis of the *J(V)* curves recorded daily, weekly, and monthly is reported in Fig. S6. The performances of the two other tandems (sample B and C) and the SHJ reference device are shown in Fig. S7. While sample B exhibits a similar trend as the one shown in Fig. 1, a failure in the edge seal of the glass-glass packaging degraded sample C after ~16 weeks, which underscores the importance of developing robust encapsulation strategies for perovskite-based solar cells.

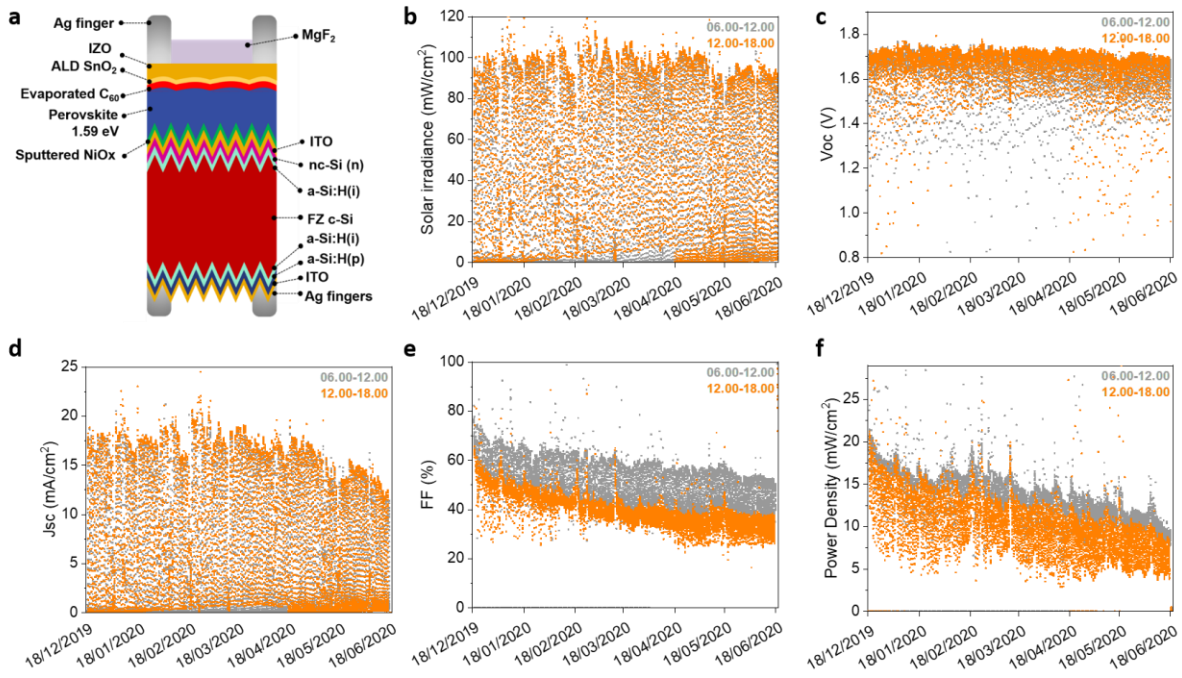

Fig. 1. Outdoor performance of perovskite/silicon tandem devices. a) Bifacial monolithic tandem layout. b) Solar irradiance measured in the outdoor test-field from the 19th Nov 2019 to the 17th Jun 2020. c-f) V_{oc}, J_{sc}, *FF*, and power density of sample A, over six months. Morning data (06:00-12:00) are highlighted in gray, while the afternoon data (12:00-18:00) are in orange. Test-field location: Jeddah, Saudi Arabia (22.302494, 39.110737).

To elucidate the mechanism behind the cyclic variation and decay in *FF*, we first compare the hourly device performances during the first and last day of our dataset. On the first day (Fig. 2a), the *FF* is highest in the early morning, gradually decreasing throughout the day. This reduction is concomitant with the rising of the ambient temperature and, hence, of the device. Towards the evening a slight increase in *FF* (~5%) can be seen, which suggests that during the day the current matching between the top and bottom cells is altered,[25,26] likely caused by variations in the albedo, resulting in higher *FF* values with increased current mismatch.[15] Such variations may have several causes, such as shadowing of the ground due to adjacent modules and mounting structures. After six months of outdoor testing, the absolute value of the *FF* is significantly reduced compared to the first day (Fig. 2b), even though qualitatively the daily trends remain similar: We find systematically that the daily decay of the *FF* recovers overnight, as shown in the trends for the first and last weeks in Fig. 2c. This overall behavior suggest that the *FF* is affected by two forms

of degradation: *i)* a decay over the day, which mostly recovers overnight, and *ii)* a steady and irreversible degradation mechanism.

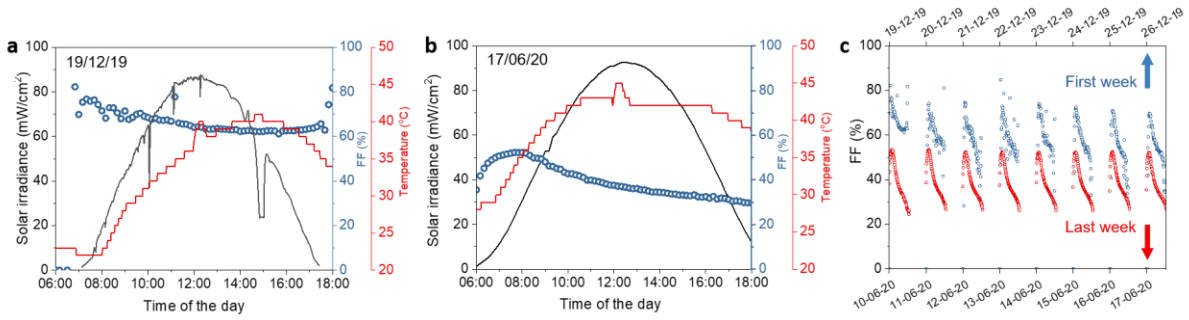

Fig. 2. Daily and weekly trends of the fill factor (FF). a) Daily trend of the FF, solar irradiance, and ambient temperature for the first day in the test field (19th of December, 2019). b) Daily trend of the FF and solar irradiance for the last day in the test field (17th Jun 2020). c) Weekly trend of the FF for the first week (blue) and last week (red) in the test-field. The blue and red arrows indicate the week time axis.

After six months in the test-field, we removed sample A to investigate the origin of the reversible degradation. We designed experiments to disentangle the effects of light, temperature, and electric field in an effort to reproduce the effects of the diurnal cycle in the controlled laboratory environment. When exposing the device to several hours of simulated sunlight in its monofacial configuration and keeping the device under open-circuit conditions (only briefly interrupted to record a *J(V)* curve every 10 minutes), we observe a similar *FF* trend as seen in the test-field (Fig. 3a). For this experiments, we measured the sample using only front irradiation as explained in the Supplementary Note, with the purpose to probe the combined effects of light and temperature. Therefore, we selected two temperatures (35 °C and 50 °C) representative of what we recorded in the test-field (Fig. S8). Further, we investigated the device performance as a function of light intensity, applying a stepwise intensity increase, matching the temporal evolution of daily solar irradiance. Fig. 3b shows the *FF* of the tandem device when cycling the AM1.5g spectrum between 10 and 100 mW/cm^2 and back to 10 mW/cm^2 to simulate a full daily cycle. As shown in Fig. 3b, the *FF* is not affected by this. This excludes variable lighting conditions in the field as the origin for the change in *FF* during the day. This experiment also excludes the effect of parasitic series

resistance induced by long-term aging, otherwise the *FF* would have increased at low irradiance. However, we cannot exclude with this experiment the presence of localized regions with high series resistances due to the degradation of the contact.[27] Moreover, we cannot exclude potential variations in the albedo, and its influence on the *FF*, as the device in the lab is irradiated only from the front side.[28,29] For a better insight, we compared the *J(V)* curves recorded in the lab experiment with the *J(V)* curves recorded in the test-field, at the same irradiation conditions (Fig. S9). Outdoor, the device presented a shunted-like behavior, which is responsible for the lower FF. Likely, this behavior is the consequence of induced localized regions with very high series resistance that originate from an alteration of the contact stack, or a potential degradation in the perovskite top-cell (see below).[27] We then probed the effect of elevated temperatures by keeping the sample at 50 °C in the dark. The dark periods were again only interrupted for periodic *J(V)* measurements with light irradiation only for the duration of the measurement. We found that the *FF* did not degrade under these circumstances, thus excluding a temperature-induced decay (Fig. 3c). However, we find that the temperature does accelerate the light-induced degradation, as shown by temperature-controlled degradation measurements at 35 °C and 50 °C (Fig. 3a).

Under real-world conditions, solar cells are rarely subject to open-circuit conditions, such as in the test-field, but will be mainly maintained near the maximum power point (MPP), generating electrical power. We therefore probed the device at a constant voltage near the MPP and tracked the stabilized power output (SPO) current for four hours in a controlled environment (25 °C, 1-Sun illumination, Fig. 3d). In this case, we find that the current density at MPP drops continuously. Since the SPO is directly linked to the *FF*, the reduction in the SPO reflects a reduction in the *FF* with a similar rate as shown in Fig. 3a when the device was kept under open-circuit conditions.

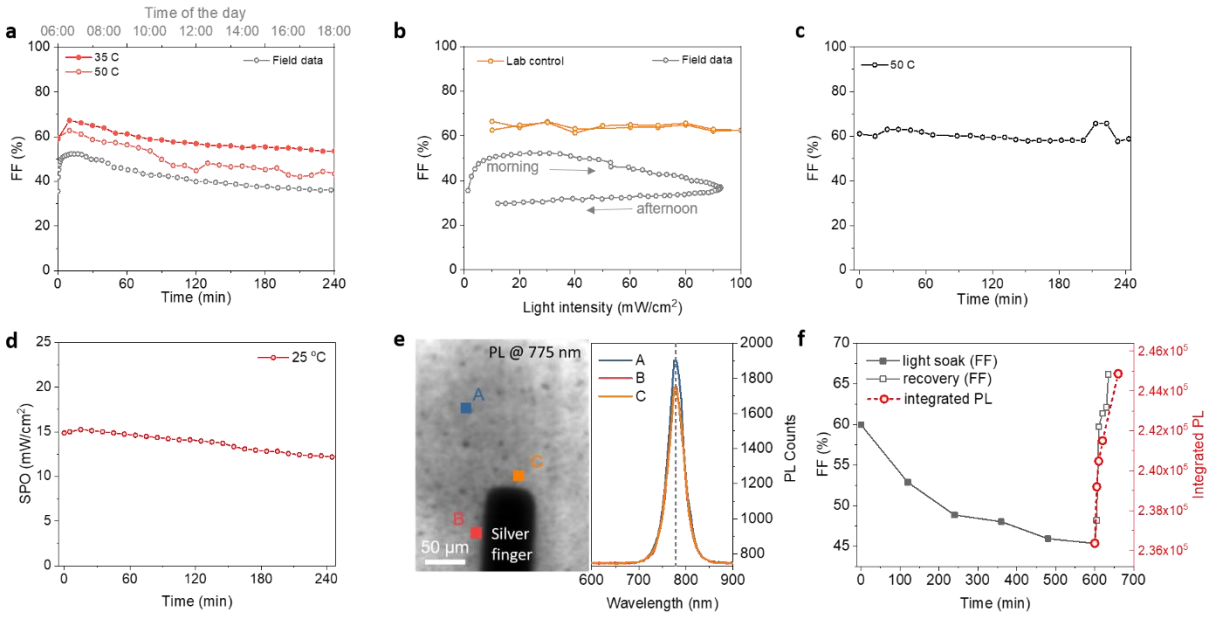

Fig. 3. Understanding the reversible degradation mechanism of Sample A. a) Variation of the *FF* over 4 hours of constant irradiation at 1-Sun at 50 °C (red, hollow circles) and 35 °C (red, full circles) compared with the field data of the last day in the test field (gray, open circles). b) Variation of the *FF* as a function of light intensity in the lab (orange), compared with the *FF* measured the last day of the test field experiment (gray). c) Effect of annealing the cell in the dark on *FF* (black circles). The annealing in the dark was interrupted every 10 min for *J(V)* measurements. d) Stabilized power output (SPO) for the device thermalized at 25 °C. e) PL mapping (left) and PL spectrum of the device at different color coded points (right). f) Comparison between *FF* and PL recovery. The sample was light-soaked at 1-Sun for 10 hours at open circuit condition, every 2 hours we performed a *J(V)* curve to evaluate the *FF* (gray squares). After the light-soaking we tracked the recovery of the *FF* by keeping the sample in dark, except for short exposures during the recording of a *J(V)* curve (gray open squares). The red circles represent the recovery time of the PL, based on its integrated values.

Overall, these experiments suggest that the reversible mechanism is induced by light exposure, which is exacerbated by temperature. Temperature and the presence of an electric field over the device stack alone do not significantly affect the *FF*. Similarly, we exclude the presence of parasitic series resistance, possibly induced by aging, as a cause for the reversible degradation, as demonstrated by low-intensity light exposure (Fig. 3b).

To further clarify the origin of the reversible degradation, we investigated the photoluminescence (PL) of the aged sample. Since the spectral shape of the steady-state PL signal is affected by the phase stability, we used it to track the nature of the reversible degradation.[30] Conversely, the *intensity* of the PL signal directly scales with the densities of free electrons and holes (which in turn depend on excitation, defect densities, and possible voltage biasing of the devices). Fig. 3e

shows a PL image taken around the silver finger electrode of sample A after the six-month experiment. The PL spectrum appears to be uniformly distributed around a maximum, centered at 778 nm, matching emission from the perovskite, without any signs of broadening or distortion due to bromide segregation for any spot probed. This phase stability confirms our expectation, considering that the perovskite (bandgap 1.59 eV) is mostly composed of iodide as halide.[23] Next, sample A was light-soaked for ten hours under 1-Sun at ~50 °C. Immediately after the light soaking, we recorded the PL signal at the same spot at different time delays. The PL intensity was quenched after light soaking, but recovered in dark gradually over time.

After overnight recovery in the dark, we light-soaked sample A again for ten hours, using the same conditions as in the PL experiment. During this light-soaking, we probed the *FF* every two hours. After ten hours of light-soaking, we measured the recovery of the *FF*, keeping the device in dark and only illuminating to record the *J(V)*-curve. In Fig. 3f, we report the dynamics of the *FF* and the PL during the experiment. The close similarity in temporal behavior of *FF* and integrated PL signal during the recovery strongly suggests a correlation between the reversible degradation in device performance and recombination in the perovskite. Considering that the V_{oc} remains mostly unchanged during 6 months it is unlikely that the bulk semiconductor becomes permanently degraded (Fig. S3a). As a consequence, the light-induced loss in PL signal (and its overnight recovery) suggests that during light soaking either metastable defects are generated or that the internal electrical field is changed, sweeping carriers away, resulting in a decrease in radiative recombination. Notably, we also found that the devices before and after light soaking show increased hysteresis in their *J(V)* characteristic (Fig. S10), which strongly suggests ion migration might play a role in the daily reversible degradation.[31,32]

The migration of ions, their relative accumulation at the interfaces, and their impact on charge extraction are well-known phenomena in perovskite semiconductors, and account for adverse effects such as hysteresis and performance roll-off of photovoltaic parameters.[33] Here, we hypothesize that a light-induced electric field drives ions to the interface during the day, thereby affecting charge extraction and causing a reduction in *FF*.[34] The effect is reversed during the night in the absence of light. The fact that initially hysteresis-free devices develop hysteresis over time is a phenomenon that needs further investigation and mitigation.

As a means to address the irreversible degradation mechanism, we subjected one of the aged devices to compositional characterization by scanning electron microscopy (SEM) and scanning transmission electron microscopy (STEM). For this analysis, we focused on the top-cell, as the SHJ bottom-cell remained stable over the course of our investigation. To do this, we carefully opened the glass/glass encapsulation of sample B. Fig. S11a displays the SEM image of the IZO surface, under the silver electrode (which was peeled-off) and a cross-sectional image (Fig. S11b). Both images show a compact and uniform perovskite film, visually identical to a freshly prepared sample (Fig. S11c). On the contrary, the silver busbar, used for contacting the device, gives evident signs of degradation with the formation of clustered structures (Fig. S12). We analyzed these structures in detail by performing a thorough STEM energy-dispersive X-ray spectroscopy (EDX) analysis of the cross-section of the device prepared using the conventional focused ion beam (FIB) lift-out method. The thin lamella was extracted from the edge of one Ag finger (see Fig. S13). Fig. 4a shows a STEM high-angle annular dark-field (HAADF) image and a corresponding EDX map of the device cross-section. After six months, each layer preserved its original thickness and uniformity without any evident alteration, except the top surface which is now covered with silver iodide (AgI_x) clusters (see arrowheads), in line with previous observations.[3] These clusters form

on the MgF_2 antireflective layer at the position of the finger grid. We also detect similar clusters directly on the Ag frame (which does not feature any MgF_2 layer), as identified by X-ray photoelectron spectroscopy (XPS) of the peeled-off electrode (Fig. S14). Overall, this indicates that over time the silver electrode gradually and irreversibly oxidizes, accounting, at least in part, for the observed irreversible *FF* degradation. To understand the mechanism controlling this process in more detail, STEM HAADF images and EDX maps were acquired at higher resolution and elemental line profiles were extracted from the latter (Fig. 4b). Three observations emerge from this analysis: *i)* the MgF_2 layer is not a dense film, but rather porous. *ii)* Ag clusters are present within the MgF_2 layer (see circled areas), suggesting that Ag migrates outwards through the MgF_2 porosity but not through the compact IZO layer towards the perovskite layer. *iii)* Iodide is present in the perovskite film and in the AgI_x clusters on the top surface, but not in the charge transport, antireflective coating or electrode layers (the small I signal in the line profile detected in the SnO_x, Ag and IZO is due to background noise). The absence of iodide in the contact and electrode layers and the absence of large voids at the top of the perovskite layer suggest that the iodide of the AgI_x does not migrate through the contact stack but comes from elsewhere, possibly from the edges of the device.[10] The IZO contact offers better barrier performances against halide migration with respect to ITO.[35] This is due to the amorphous nature of IZO, which does not require any further post-deposition annealing and forms a denser layer than crystalline ITO.

In parallel to the analysis of the silver layer, we investigated the C_{60} electron transport layer more closely. Fullerenes are well known within the organic photovoltaics (OPV) community for their morphological instabilities leading to bulk recombination phenomena.[36,37] Indeed, fullerenes tend to spontaneously aggregate in the bulk heterojunction of OPV devices by forming crystalline domains that can be hundreds of nanometers in diameter.[38,39] This aggregation is accentuated in

the presence of temperature. To investigate if C_{60} aggregation is a possible degradation mechanism in stressed tandem devices, we prepared two test samples by evaporating 40 nm C_{60} on top of the perovskite layer (all the bottom layers are those of the tandem configuration). The topography of one sample (pristine) is immediately analyzed using atomic force microscopy (AFM), while the other (aged) is glass/glass laminated and exposed in the test field for three weeks. The AFM image of the pristine sample (Fig. S15a) shows the typical morphology of the perovskite grains, with C_{60} features evident in high resolution (see Fig. S16). Conversely, the surface topography of the aged sample (Fig. S15b) is dominated by spherical clusters with different heights of up to 100 nm, with the perovskite morphology unchanged underneath. Notably, in these test samples, the absence of the top layers (SnO_x buffer layer, IZO TCO) may favor the aggregation of C_{60}. Still, these experiments reveal a possible mechanism of irreversible degradation of the electron-contact stack that may limit not only the charge extraction, hence the *FF*, but also it may limit the current itself, as shown in Fig. S4. This type of degradation is typical of the perovskite top-cell. Therefore, we analyzed the electrical behavior of each sub-cell independently, with a similar approach to Jŏst *et al.*;[40] we confirmed that this contact degradation affects severely the top-cell with a shunted behavior (see Fig. S17), in line with a modification of the extraction properties of the C_{60} layer.

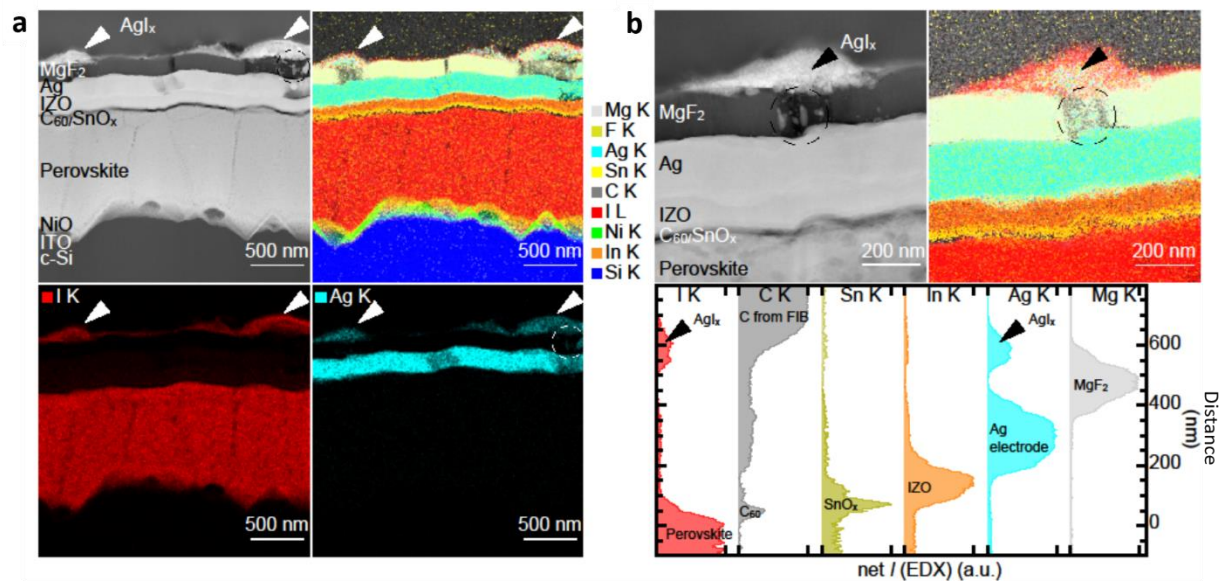

Fig. 4. Structural characterization of the tandem after six months of test-field. a) STEM HAADF image and EDX map of the overall morphology of the device after aging. b) Analysis of the front side of the cell by STEM HAADF imaging, EDX mapping and a corresponding line profile tracking the evolution of the net intensity of a selection of EDX peaks across the layer stack (after background subtraction and peak deconvolution using the Bruker Esprit software). Not that the I L edge was used for maps, while the K edge was used when computing line profiles (to facilitate the deconvolution with the Cs L edges). Arrowheads highlight the formation of AgI_x clusters on the top surface, while circled regions show metallic Ag clusters in the MgF_2.

Lab-scale perovskite/silicon tandem devices are often realized in designs aimed at maximizing the PCE rather than focusing on stability. For example, several layers (perovskite, C_{60}, ALD-SnO_x) cover the complete substrate uniformly. Others (IZO, Ag, and MgF_2) are deposited through a shadow mask to define the device-active area that is often only a small part of a larger substrate (here, the larger silicon wafer, into which the silicon bottom cell is defined by its TCO-based contacts).[7] For this reason, a significant region outside the active area is not covered by the protective barrier offered by the IZO. These unprotected areas can be subject to sublimation of the iodide from the perovskite layer.[41] Shi *et al.* recently showed that iodide sublimation is among the primary causes of degradation in a vacuum-laminated perovskite-based device, similar to the encapsulated devices presented here.[10,34] Particularly, the sublimated iodine can react with the top

silver contact (bus-bar), and the silver migrated through the MgF_2, enabling the mechanism described above.

This type of iodine migration could be resolved by several strategies. The first approach is to directly inhibit iodine sublimation. This is possible by scaling up the active area thus eliminating the presence of an exposed perovskite layer. On an industrial scale, this is anyways a necessary requirement to minimize geometrical losses. The second approach involves the lamination process. Similar to silicon modules, industrial perovskite/silicon modules will likely include two layers of encapsulant materials (such as EVA or POE) to provide the necessary mechanical integrity of interconnected tandem solar cells. The encapsulant layers provide a barrier for iodine sublimation and simultaneously act as an anti-reflective coating.[10] The last approach involves to preventing the aggregation of the C_{60} layer. While this approach does not limit the ion migration and its effects, preventing the aggregation of C_{60} can favor the stability against the irreversible degradation. This could be realized by chemically modifying the C_{60} or replacing it altogether. In the past, derivatives of C_{60}, *e.g.*, C_{60} dimers and side-chain functionalized fullerenes, haven been shown to successfully inhibit aggregation. Moreover, the OPV community has developed many high-efficiency n-type non-fullerene semiconducting monomer units. The introduction of these solution-processable molecules in tandem devices remains largely unexplored but represents an opportunity to further enhance the *FF* and stability of these devices.

We have shown the performance of bifacial perovskite/silicon tandem solar cells over six months in an outdoor environment. The *FF* is the parameter mainly responsible for the observed performance loss, while the V_{oc} and J_{sc} preserve their initial values. We identified two mechanisms that affect the *FF*: a reversible degradation that reduces the *FF* on a daily basis, recovering overnight, and an irreversible degradation that steadily reduces the maximum values of the *FF*.

We assign the root cause of the reversible mechanism to ion migration and relative interface modification, enabled by a combination of light and temperature. We identified the irreversible mechanism with the silver top electrode's alteration, combined with alteration of the C_{60} contact. Finally, we presented several strategies to resolve these issues. These strategies are collectively an intrinsic part of the improvement process that perovskite/silicon tandems have to face towards their commercialization: scaling-up, and encapsulation.

ACKNOWLEDGMENTS

This work supported by the King Abdullah University of Science and Technology (KAUST) Office of Sponsored Research (OSR) under award no. OSR-2018-CPF-3669.02, KAUST OSR-CARF URF/1/ 3079-33-01, KAUST OSR-CRG RF/1/3383, KAUST OSR-CRG2018-3737, and IED OSR-2019-4208. This work was supported in part by the US Department of the Navy, Office of Naval Research (grant award no. N00014-20-1-2572). Financial support from the Swiss Federal Office of Energy (SI/501804-01 INTENT), the Swiss National Science Foundation (176552 Bridge Power, CRSII5_171000 Sinergia Episode) is acknowledged.

SUPPORTING INFORMATION

Experimental part; J(V) curves of the bifacial tandems measured before and after encapsulation under standard condition and in the first day in the test-field; environmental humidity; Voc and Jsc variation after six-months, temperature monitoring of a tandem device, ambient temperature, and current trend; FF variation on single junction perovskite solar cells in the test-field; analysis of the J(V) curves of sample A recorded during the outdoor experiment; test-field performances of the tandems and the silicon heterojunction reference over six months; supplementary note: laboratory setup for lab experiments; temperature for a device in the outdoor; comparison between J(V) curves at different light intensities; hysteresis before and after the test-field experiment; Scanning Electron Microscopy images of aged, fresh perovskite, and silver electrode; lamella for the TED-EDX analysis; X-ray Photoelectron Spectroscopy analysis of the silver electrode; Atomic Force Microscopy of C60 on the perovskite film on a pristine and aged samples; Sub-cell performances of Sample A.

REFERENCES

1 Haegel, N. M. *et al.* Terawatt-scale photovoltaics: Transform global energy. *Science* **364**, 836-838 (2019).
2 Xu, J. *et al.* Triple-halide wide–band gap perovskites with suppressed phase segregation for efficient tandems. *Science* **367**, 1097-1104 (2020).
3 Sahli, F. *et al.* Fully textured monolithic perovskite/silicon tandem solar cells with 25.2% power conversion efficiency. *Nature Materials* **17**, 820-826, doi:10.1038/s41563-018-0115-4 (2018).
4 Kim, D. *et al.* Efficient, stable silicon tandem cells enabled by anion-engineered wide-bandgap perovskites. *Science* **368**, 155-160 (2020).
5 Hou, Y. *et al.* Efficient tandem solar cells with solution-processed perovskite on textured crystalline silicon. *Science* **367**, 1135-1140 (2020).
6 Bush, K. A. *et al.* 23.6%-efficient monolithic perovskite/silicon tandem solar cells with improved stability. *Nature Energy* **2**, 17009, doi:10.1038/nenergy.2017.9

https://www.nature.com/articles/nenergy20179#supplementary-information (2017).
7 Al-Ashouri, A. *et al.* Monolithic perovskite/silicon tandem solar cell with> 29% efficiency by enhanced hole extraction. *Science* **370**, 1300-1309 (2020).
8 (NCPV), N. N. C. f. P. (2020).
9 Jošt, M., Kegelmann, L., Korte, L. & Albrecht, S. Monolithic Perovskite Tandem Solar Cells: A Review of the Present Status and Advanced Characterization Methods Toward 30% Efficiency. *Advanced Energy Materials*, 1904102 (2020).
10 Shi, L. *et al.* Gas chromatography–mass spectrometry analyses of encapsulated stable perovskite solar cells. *Science* (2020).
11 Divitini, G. *et al.* In situ observation of heat-induced degradation of perovskite solar cells. *Nature Energy* **1**, 1-6 (2016).
12 Leijtens, T. *et al.* Stability of metal halide perovskite solar cells. *Advanced Energy Materials* **5**, 1500963 (2015).
13 Berhe, T. A. *et al.* Organometal halide perovskite solar cells: degradation and stability. *Energy & Environmental Science* **9**, 323-356 (2016).
14 Khenkin, M. V. *et al.* Consensus statement for stability assessment and reporting for perovskite photovoltaics based on ISOS procedures. *Nature Energy* **5**, 35-49 (2020).
15 Aydin, E. *et al.* Interplay between temperature and bandgap energies on the outdoor performance of perovskite/silicon tandem solar cells. *Nature Energy*, 1-9 (2020).
16 Jošt, M. *et al.* Perovskite Solar Cells go Outdoors: Field Testing and Temperature Effects on Energy Yield. *Advanced Energy Materials*, 2000454.
17 Cheacharoen, R. *et al.* Encapsulating perovskite solar cells to withstand damp heat and thermal cycling. *Sustainable Energy & Fuels* **2**, 2398-2406 (2018).
18 Hoke, E. T. *et al.* Reversible photo-induced trap formation in mixed-halide hybrid perovskites for photovoltaics. *Chemical Science* **6**, 613-617 (2015).
19 Domanski, K. *et al.* Not all that glitters is gold: metal-migration-induced degradation in perovskite solar cells. *ACS nano* **10**, 6306-6314 (2016).
20 Fu, F. *et al.* I 2 vapor-induced degradation of formamidinium lead iodide based perovskite solar cells under heat–light soaking conditions. *Energy & Environmental Science* **12**, 3074-3088 (2019).
21 Duong, T. *et al.* Light and elevated temperature induced degradation (LeTID) in perovskite solar cells and development of stable semi-transparent cells. *Solar Energy Materials and Solar Cells* **188**, 27-36 (2018).
22 Reyna, Y. *et al.* Performance and stability of mixed FAPbI3 (0.85) MAPbBr3 (0.15) halide perovskite solar cells under outdoor conditions and the effect of low light irradiation. *Nano Energy* **30**, 570-579 (2016).
23 De Bastiani, M. *et al.* Efficient bifacial monolithic perovskite/silicon tandem solar cells via bandgap engineering. *Nature Energy*, doi:10.1038/s41560-020-00756-8 (2021).
24 Cheacharoen, R. *et al.* Design and understanding of encapsulated perovskite solar cells to withstand temperature cycling. *Energy & Environmental Science* **11**, 144-150 (2018).
25 Köhnen, E. *et al.* Highly efficient monolithic perovskite silicon tandem solar cells: analyzing the influence of current mismatch on device performance. *Sustainable Energy & Fuels* **3**, 1995-2005 (2019).
26 Ameri, T., Dennler, G., Lungenschmied, C. & Brabec, C. J. Organic tandem solar cells: A review. *Energy & Environmental Science* **2**, 347-363 (2009).
27 Sugianto, A. *et al.* Impact of localized regions with very high series resistances on cell performance. *Progress in Photovoltaics: Research and Applications* **20**, 452-462, doi:https://doi.org/10.1002/pip.1163 (2012).

28 Boccard, M. & Ballif, C. Influence of the Subcell Properties on the Fill Factor of Two-Terminal Perovskite–Silicon Tandem Solar Cells. *ACS Energy Letters* **5**, 1077-1082 (2020).
29 Onno, A. *et al.* Predicted Power Output of Silicon-Based Bifacial Tandem Photovoltaic Systems. *Joule* (2020).
30 Brennan, M. C., Ruth, A., Kamat, P. V. & Kuno, M. Photoinduced anion segregation in mixed halide perovskites. *Trends in Chemistry* **2**, 282-301 (2020).
31 De Bastiani, M. *et al.* Interfacial dynamics and contact passivation in perovskite solar cells. *Advanced Electronic Materials* **5**, 1800500 (2019).
32 Holovský, J. *et al.* Lead Halide Residue as a Source of Light-Induced Reversible Defects in Hybrid Perovskite Layers and Solar Cells. *ACS Energy Letters* **4**, 3011-3017 (2019).
33 Domanski, K. *et al.* Migration of cations induces reversible performance losses over day/night cycling in perovskite solar cells. *Energy & Environmental Science* **10**, 604-613, doi:10.1039/C6EE03352K (2017).
34 Tan, S. *et al.* Shallow Iodine Defects Accelerate the Degradation of α-Phase Formamidinium Perovskite. *Joule* **4**, 2426-2442 (2020).
35 Boyd, C. C. *et al.* Barrier design to prevent metal-induced degradation and improve thermal stability in perovskite solar cells. *ACS Energy Letters* **3**, 1772-1778 (2018).
36 Li, Z. *et al.* Performance enhancement of fullerene-based solar cells by light processing. *Nature Communications* **4**, 2227, doi:10.1038/ncomms3227 (2013).
37 Piersimoni, F. *et al.* Influence of fullerene photodimerization on the PCBM crystallization in polymer: fullerene bulk heterojunctions under thermal stress. *Journal of Polymer Science Part B: Polymer Physics* **51**, 1209-1214 (2013).
38 Heumueller, T. *et al.* Morphological and electrical control of fullerene dimerization determines organic photovoltaic stability. *Energy & Environmental Science* **9**, 247-256 (2016).
39 Wu, W.-R. *et al.* Competition between fullerene aggregation and poly (3-hexylthiophene) crystallization upon annealing of bulk heterojunction solar cells. *Acs Nano* **5**, 6233-6243 (2011).
40 Jošt, M. *et al.* Subcell Operation and Long-Term Stability Analysis of Perovskite-Based Tandem Solar Cells Using a Bichromatic Light Emitting Diode Light Source. *Solar RRL* **n/a**, 2100311, doi:https://doi.org/10.1002/solr.202100311.
41 Ugur, E. *et al.* How Humidity and Light Exposure Change the Photophysics of Metal Halide Perovskite Solar Cells. *Solar RRL* **4**, 2000382 (2020).